Radial transport of poloidal momentum in ASDEX Upgrade in L-mode and H-mode

F. Mehlmann[1], R. Schrittwieser[1], V. Naulin[2], J.J. Rasmussen[2], H.W. Müller[3], C. Ionita[1], A.H. Nielsen[2], N. Vianello[4], V. Rohde[3], ASDEX Upgrade Team[3]

[1]*Institute for Ion Physics and Applied Physics, EURATOM-ÖAW Association, University of Innsbruck, Austria*

[2]*Association EURATOM – DTU, Technical University of Denmark, Department of Physics, DTU Risø Campus, Roskilde, Denmark*

[3]*Max-Planck-Institute for Plasma Physics, EURATOM Association, Garching, Germany*

[4]*Consorzio RFX, Associazione Euratom-ENEA sulla Fusione, Padova, Italy*

Abstract: A reciprocating probe was used for localized measurements of the radial transport of poloidal momentum in the scrape-off layer (SOL) of ASDEX Upgrade (AUG). The probe measured poloidal and radial electric field components and density. We concentrate on three components of the momentum transport: Reynolds stress, convective momentum flux and triple product of the fluctuating components of density, radial and poloidal electric field. For the evaluation we draw mainly on the probability density functions (PDFs).

1. Introduction

The radial flux of poloidal momentum was investigated in the SOL of ASDEX Upgrade (AUG) by a probe head carrying six cold probe pins [1]. Four pins were electrically floating to derive the poloidal and radial electric field components $E_{\theta,r}$, one pin was negatively biased to determine the density n. The probe head was mounted on the midplane manipulator and inserted during the diverted period of L-mode discharge #23157 and H-mode discharge #23163 for 100 ms in each case. The discharge parameters are summarized in Table I. Even though the reliability of this method to measure electric fields is debatable, it is yet the only one applicable from the start of the probe insertion. Naturally, emissive probes would be preferable, but self-emission is no option since it takes several ms until the probes become uniformly self-emissive, if at all, which depends also on the depth of insertion (see e.g. [2]).

The radial flux of poloidal momentum reads: $M_r = nv_r v_\theta = nE_\theta E_r / B_\phi^2$ ($v_{r,\theta} = E_{\theta,r}/B_\phi$, B_ϕ is the toroidal magnetic field). With n and the radial and poloidal velocity components, $v_{r,\theta}$, defined as $X = X_0 + X_{\mathrm{fl}}$ (stationary and fluctuating component, respectively), M_r splits into various contributions [3,4]. We discuss the probability density functions (PDF) of the total momentum flux M_r and its three non-zero components: (i) Reynolds stress $\mathcal{R}e = n_0 v_{r,\mathrm{fl}} v_{\theta,\mathrm{fl}}$, (ii) triple fluctuating product $n_{\mathrm{fl}} v_{r,\mathrm{fl}} v_{\theta,\mathrm{fl}}$ and (iii) convective momentum $v_{\theta,0}\Gamma = v_{\theta,0} n_{\mathrm{fl}} v_{r,\mathrm{fl}}$.

Table I. Plasma current I_{pl}, electron density n_e, total magnetic field B_t, neutral beam injection power P_{NBI}, ion cyclotron resonance heating power P_{ICRH}, safety factor q_{95} and minimum distance from last closed flux surface (LCFS) for the two discharges discussed here.

Shot #	I_{pl} (MA)	n_e (m^{-3})	B_t (T)	P_{NBI} (MW)	P_{ICRH} (MW)	q_{95}	l_{min} (mm)
L-mode #23157	0,8	$4{,}9\cdot10^{19}$	–2,48			5,26	45
H-mode #23163	0,8	$6{,}7\cdot10^{19}$	–2,48	5,1	3,7	5,25	38

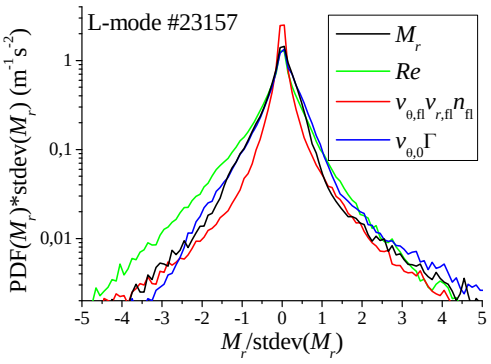

Fig. 1: PDFs of the total momentum transport M_r (black line), and of the three components during the diverted L-mode discharge #23157: Reynolds stress $\mathcal{Re}$ (olive line), triple fluctuating product $n_{fl}\,v_{r,fl}\,v_{\theta,fl}$ (red line), convective momentum flux $v_{\theta,0}\Gamma$ (blue line). insertion time interval t = 2,195-2,295 s.

The statistical spread of the data was usually very strong. Therefore it is problematic to obtain reasonable values for the higher statistical moments (skewness and kurtosis). Deriving a PDF means dividing the data series into cells and counting the hits in each cell. However, in the wings of the distribution only few points are left. So the statistics of big numbers cannot be applied any more. To overcome this problem a rule was defined: When 5 neighbouring cells have less than 5 hits, these cells are ignored. The hits in the cells and thereby the limits can be varied more or less arbitrarily by varying the cell size. To avoid arbitrariness as far as possible, we have chosen a constant cell size of 0,1·FWHM (Full Width Half Maximum) of the distributions. The PDFs are normalized to the standard deviations (stdev). These very complex questions will be treated in a forthcoming long paper [5].

2. Experimental results and discussion

Fig. 1 shows the PDFs of the total transport of momentum M_r and of the three above mentioned components for L-mode discharge #23157. Table II contains mean values, standard deviations, skewnesses and kurtoses of the data series.

Table II: Mean values, standard deviation (stdev), skewness and kurtosis of the total flux of momentum M^r and its three components Reynolds stress $\mathcal{Re}$, triple fluctuating product $n_{fl}\,v_{r,fl}\,v_{\theta,fl}$ and convective momentum $v_{\theta,0}\Gamma = v_{\theta,0}n_{fl}v_{r,fl}$ for L-mode discharge #23157.

L-mode #23157	Mean value	Stdev	Skewness	Kurtosis
M_r	$7{,}27\cdot10^{20}$	$20{,}73\cdot10^{21}$	3,37	42,14
$\mathcal{Re}$	$-9{,}02\cdot10^{20}$	$9{,}25\cdot10^{21}$	-0,85	20,90
$n_{fl}\,v_{r,fl}\,v_{\theta,fl}$	$2{,}91\cdot10^{20}$	$6{,}87\cdot10^{21}$	2,99	73,49
$v_{\theta,0}\Gamma$	$13{,}01\cdot10^{20}$	$12{,}61\cdot10^{21}$	3,50	34,71

In case of H-mode discharge #23163 (see Fig. 2), M_r and its three components were also calculated separately for ELM-intervals and inter-ELM intervals, i.e. all ELM intervals and all inter-ELM intervals were concatenated separately. Fig. 2(a) shows the PDFs for the entire H-mode, (b) for the inter-ELM in-

tervals and (c) for the ELM intervals. Table III indicates the corresponding mean values, standard deviations, skewnesses and kurtoses of the data series.

Fig. 1 of the L-mode discharge shows rather symmetric PDFs with that of the Reynolds stress showing the highest symmetry, a negative mean value and a slightly negative skewness. All other PDFs show positive skewness.

The PDFs of the entire H-mode discharge (Fig. 2(a)) show a similar behaviour. Also in this case the Reynolds stress shows the most symmetric distribution, with low, however positive values of mean and skewness. The PDFs of the other three components are strongly positively skewed for values of M_r/stdev(M_r) > 2. This is also reflected in their skewness values (Table III(a)). The PDFs of Fig. 2(b) (inter-ELM intervals) are all relatively symmetric with that of the convective term most bulging, i.e. most positively skewed in the range of

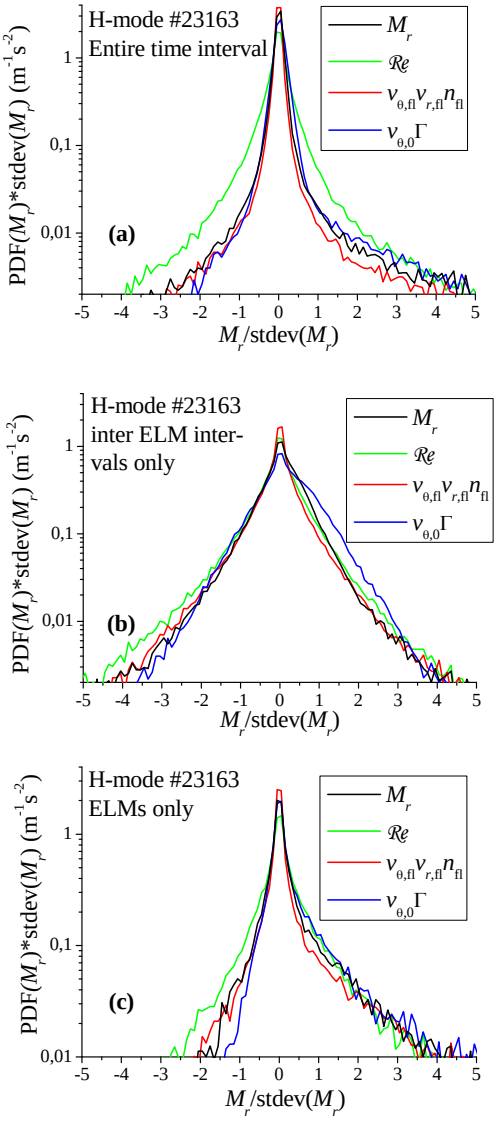

Fig. 2. PDFs of the total momentum transport M_r (black line) and of the three components for H-mode discharge #23163, for the entire H-mode (a), during the inter-ELM intervals (b) and during the ELM intervals (c): Reynolds stress $\mathcal{R}e$ (green line), triple fluctuating product $n_{fl}\,v_{r,fl}\,v_{\theta,fl}$ (red line), convective momentum flux $v_{\theta,0}\Gamma$ (blue line), t = 2,970-3,070 s.

Table III: Mean values, standard deviation (stdev), skewness and kurtosis of the total flux of momentum M^r and its three components Reynolds stress $\mathcal{R}e$, triple fluctuating product $n_{fl}\,v_{r,fl}\,v_{\theta,fl}$ and convective momentum $v_{\theta,0}\Gamma = v_{\theta,0}n_{fl}v_{r,fl}$ for the entire H-mode discharge #23163 (a), for the concatenated inter-ELM intervals (b) and the concatenated ELM intervals (c).

(a) Entire H-mode	Mean value	Stdev	Skewness	Kurtosis
M_r	$1{,}12\cdot10^{23}$	$11{,}36\cdot10^{23}$	8,31	107,41
$\mathcal{R}e$	$0{,}16\cdot10^{23}$	$3{,}78\cdot10^{23}$	3,56	56,57
$n_{fl}\,v_{r,fl}\,v_{\theta,fl}$	$0{,}33\cdot10^{23}$	$4{,}79\cdot10^{23}$	7,71	111,99
$v_{\theta,0}\Gamma$	$0{,}68\cdot10^{23}$	$4{,}45\cdot10^{23}$	9,01	106,05
(b) Inter-ELMs				
M_r	$13{,}76\cdot10^{21}$	$2{,}01\cdot10^{23}$	0,81	38,04
$\mathcal{R}e$	$-2{,}11\cdot10^{21}$	$1{,}66\cdot10^{23}$	-0,18	14,51
$n_{fl}\,v_{r,fl}\,v_{\theta,fl}$	$-0{,}39\cdot10^{21}$	$0{,}64\cdot10^{23}$	0,14	44,47
$v_{\theta,0}\Gamma$	$16{,}62\cdot10^{21}$	$0{,}86\cdot10^{23}$	2,02	32,91
(c) ELMs				
M_r	$8{,}52\cdot10^{23}$	$3{,}08\cdot10^{24}$	2,62	10,33
$\mathcal{R}e$	$1{,}43\cdot10^{23}$	$0{,}97\cdot10^{24}$	1,33	7,24
$n_{fl}\,v_{r,fl}\,v_{\theta,fl}$	$2{,}77\cdot10^{23}$	$1{,}34\cdot10^{24}$	2,35	10,56
$v_{\theta,0}\Gamma$	$4{,}38\cdot10^{23}$	$1{,}18\cdot10^{24}$	2,93	10,47

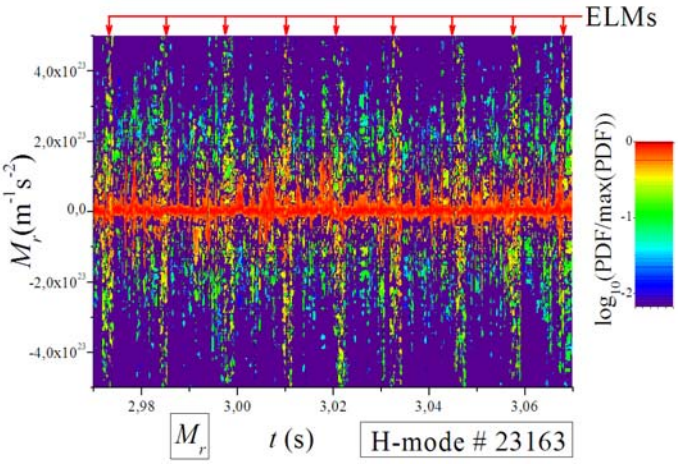

Fig. 3. Temporal evolution of the PDF of the absolute values of the total radial transport M_r of poloidal momentum during H-mode shot #23163.

$M_r/\mathrm{stdev}(M_r) \cong 1 - 2$ (see also Table III(b)). Thus between ELMs the momentum transport appears to be dominated mainly by convection. Expectedly during ELMs (Fig. 2(c)) we find the most strongly skewed PDFs for M_r and all three of its components, corresponding to the relatively large skewnesses in Table III(c). However, most of the transport occurs in the range of $M_r/\mathrm{stdev}(M_r) > 1$ which does not contribute so much to the skewness momentum. A more comprehensive treatment of these effects will be presented in [5].

As a descriptive example, Fig. 3 shows the temporal evolution of the PDF of the total radial transport of poloidal momentum M_r (absolute values) during the entire insertion of the probe head in case of H-mode shot #23163. The colour code shows increasing relative amplitude from violet to red from $6 \cdot 10^{-3}$ to 1. The ELMs are recognizable by their much broader PDFs and are marked by red arrows.

Eventually we point out that in H-mode, due to the NBI, there is an external source for toroidal angular momentum. However, in an ohmic L-mode discharge there can only be intrinsic rotation, in which case the momentum should basically be generated from turbulence in the form of residual stresses (asymmetry flows) by the Reynolds stress and direct interaction with the SOL flows.

Acknowledgements

This work, supported by the European Communities under the Contracts of Associations between EURATOM and ÖAW, IPP, ENEA-RFX and DTU, was carried out within the framework of the EFDA. The content of the publication is the sole responsibility of its authors and it does not necessarily represent the views of the Commission or its services. This work was also supported by grant P19901 of the Austrian Science Fund (FWF).

References

[1] C. Ionita, N. Vianello, H.W. Müller, et al., J. Plasma Fusion Res. Series 8, 413 (2009).

[2] B. Nold, T.T. Ribeiro, M. Ramisch, et al., New J. Phys. (2012), accepted.

[3] F. Mehlmann, C. Ionita, V. Naulin, et al., 37th EPS Conf. Plasma Phys. (Dublin, 2010), P1.1064.

[4] J. R. Myra, D. A. Russell, D.A. D'Ippolito, Phys. Plasmas 15, 032304 (2008).

[5] F. Mehlmann, V. Naulin, C. Ionita, et al., in preparation.